IEEE Access
Multidisciplinary | Rapid Review | Open Access Journal

Received September 18, 2019, accepted October 8, 2019, date of publication October 11, 2019, date of current version October 25, 2019.

Digital Object Identifier 10.1109/ACCESS.2019.2947094

A Quad-Band Dual-Sense Circularly-Polarized Square-Ring Antenna for Multi-Functional Wireless Applications

TU TUAN LE AND TAE-YEOUL YUN, (Member, IEEE)
Department of Electrical and Computer Engineering, Hanyang University, Seoul 133-791, South Korea

Corresponding author: Tae-Yeoul Yun (taeyeoul@hanyang.ac.kr)

This work was supported in part by the National Research Foundation of Korea under Grant 2018R1A5A7025522.

ABSTRACT A quad-band dual-sense circularly-polarized (CP) antenna is presented for multi-functional wireless applications. Initially, the corner-fed square-ring radiator is designed with one end open-circuited. The surface currents flow along the circumference of the square-ring, which excite dual-band dual-sense CP radiation with a right-hand circular polarization (RHCP) at one frequency band and a left-hand circular polarization (LHCP) at the other band. Later, a rhombic-shaped slot and an inverted V-shaped parasitic element, used to balance the surface currents in horizontal and vertical directions at the middle and low frequency regions, excite two additional LHCP bands. The proposed antenna is systematically presented through a CP generation principle, a surface current distribution, and parametric analysis. The measured results yield an impedance bandwidth (IBW) of 83.9% (2.33-5.70 GHz) and the 3-dB axial ratio bandwidths (ARBWs) of 7.3% (2.38-2.56 GHz), 9.0% (2.75-3.03 GHz), 3.7% (3.42-3.53 GHz), and 7.1% (5.16-5.54 GHz). The maximum broadside gains achieved within the axial ratio bandwidths are 2.5, 2.9, 3.4, and 2.7 dBi, respectively. Compared to other reported works considering quad-band CP radiation, the proposed antenna achieves a wider ARBW and smaller size. To the best of the author's knowledge, the proposed work is the first paper presenting a planar quad-band dual-sense CP antenna for WLAN (2.5/5.3 GHz), WiMAX (3.5 GHz), and Marine Service (3.0 GHz) wireless applications.

INDEX TERMS Antenna, bi-directional, circular polarization, CP, parasitic element, quad-band.

I. INTRODUCTION

A single antenna with multi-band or broadband characteristic that can operate for various wireless communication bands is significantly in demand. However, it has been known that one of the notable drawbacks of broadband antennas is interference with other radio communication systems. Circularly-polarized (CP) antennas have been widely used in the modern wireless systems. Therefore, the antenna design with multi-band circularly-polarized radiation has consequently become extremely attractive. Numerous triple-band CP antennas have been published with various types of structures: inverted U-shaped monopole [1], Y-shaped monopole [2], slot antenna [3], and stacked patch antenna [4]. To increase the number of CP bands, a triple-band CP antenna in [1] is further improved by placing over a frequency selective surface (FSS) [5]. The FSS structure was used to convert linearly polarized (LP) signals into CP signals resulting in a quad-band CP antenna. However, the FSS layer makes the antenna profile large. To solve this issue, a stacked patch antenna fed by capacitive coupling was presented [6]. However, this antenna achieved a quite narrow axial ratio bandwidth (ARBW). The antenna structure also required an air gap between the lower patch and ground plane thus increasing the antenna profile and creating complexity in fabrication process. The planar printed antenna, with its advantages of light weight, diversity of shape, and easy integration with circuits, has been popularly used in many modern wireless systems. To meet the additional requirement for some polarization diversity systems, the dual-sense CP antenna is proposed.

Numerous studies addressing the planar antenna with dual-band dual-sense CP characteristic have recently been presented. To this end, slot and monopole structures have been used in various configurations [7]–[10], i.e., coplanar waveguide-fed monopole [7], square-slot [8], spiral slot [9], and tilted D-shaped monopole [10]. These dual-sense CP antennas achieved wide dual-band ARBW. To further

The associate editor coordinating the review of this manuscript and approving it for publication was Sandra Costanzo.

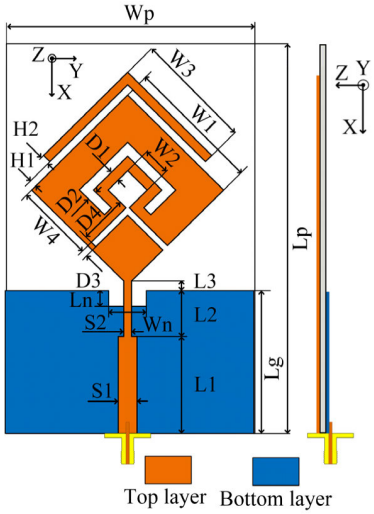

FIGURE 1. Geometry of the proposed antenna.

increase the number of CP bands, a method using square-slot and L-shaped radiator has been presented for triple-band dual-sense CP characteristics [11]. In terms of multi-band dual-sense CP antennas, the number of CP bands is, however, limited to three.

In this paper, a planar quad-band dual-sense CP antenna is proposed. The proposed antenna with its configuration properties is featured to have balanced surface currents in horizontal and vertical directions. Firstly, a simple open-loop square-ring radiator generates two CP modes. Later, a rhombic-shaped slot and an inverted V-shaped parasitic strip are introduced to excite two other CP modes. The proposed design has a simple structure and a wide ARBW at four distinct CP bands on a single substrate layer for ease of fabrication and low cost, in contrast to other previous designs. The details of the antenna design procedure, CP radiation mechanism, current distributions, and measured results are discussed in the following sections.

II. ANTENNA DESIGN AND ANALYSIS

Fig. 1 shows configuration of the proposed quad-band dual-sense circularly polarized antenna which was printed on a $75 \times 65 \times 1.52$ mm^3 Taconic TLY-5 substrate with dielectric constant of 2.2 and loss tangent of 0.009. The antenna structure is comprised of an opened-loop square-ring radiator, a rhombic-shaped slot, an inverted V-shaped parasitic strip, and a notched ground plane. A 50-Ω transmission line with an impedance transformer is used to feed the antenna. The proposed antenna is simulated by a commercial high frequency electromagnetic field simulation (HFSS) tool.

The design procedure and CP excitation principle are explained by classifying into two stages: Stage A and Stage B. Stage A presents a dual-band dual-sense CP antenna and Stage B presents a rhombic-slot and inverted V-shaped parasitic strip that can create two additional CP modes.

To explain the CP mechanism for each stages, the comparisons of simulated results with regard to IBW, amplitude ratio

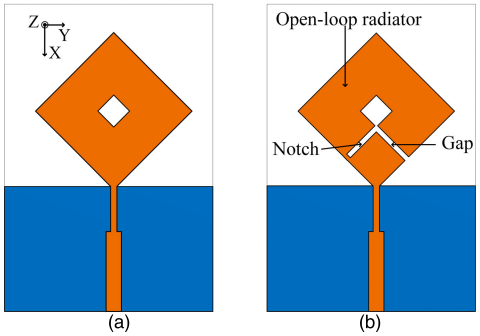

FIGURE 2. Antenna structure variations in Stage A for the first two CP-mode generation: (a) Ant1, (b) Ant2.

($|E_x|/|E_y|$) (APR), phase difference ($\angle E_x$- $\angle E_y$) (PD), and ARBW are introduced. To generate efficient CP radiation at a given frequency, the two complex valued E-field components, E_x and E_y, which have quadrature phase difference, should be orthogonal in direction and equal in amplitude:

1. The amplitude ratio $(|E_x|/|E_y|) = 0$ dB.
2. The phase difference $(\angle E_x - \angle E_y) = \pm 90^o$.

The CP operation and the sense of polarization are visualized based on the surface current distribution [12]–[14], which are qualitatively analyzed by a commercial electromagnetic field simulation tool. The parametric study is also presented to observe the influence of antenna parameters on each CP modes.

A. STAGE A

Fig. 2 shows antenna structure variations which will be discussed in Stage A: a corner-fed closed-loop square-ring antenna (Ant1) and a corner-fed opened-loop square-ring antenna (Ant2).

Ant1: linearly-polarized corner-fed closed-loop square-ring antenna

In Fig. 2 (a), the proposed antenna was initially designed with a corner-fed closed-loop antenna (Ant1). Ant1 has a fundamental mode TM_{11} [15] at a resonant frequency of around 4.8 GHz as shown in Fig. 3 (a). The surface currents are strongly distributed on the outer circumference of the square-ring with a slant angle of 45^o as shown in Fig. 4 (a). Note that the E-field component exists only in the vertical direction (x) whereas the horizontal (y) components are canceled out. This results in a very large APR of approximately 25 dB at 4.8 GHz as shown in Fig. 3 (b). Thus, Ant1 radiates linearly-polarized waves where AR $>$ 30 dB as shown in Fig. 3 (d).

***Ant2*:** dual-band dual-sense corner-fed open-loop square-ring antenna

In this antenna (Ant2), a notch and a gap are each loaded onto at two radiating arms producing an open-loop square-ring antenna, as shown in Fig. 2 (b). To understand each role of the notch and gap on the CP excitation, Ant1 with the gap only, namely as Ant1*, is investigated in Fig. 3. By inserting the gap, additional resonant modes are excited at frequencies of 2.8 and 3.7 GHz, thus achieving a wide IBW as shown in Fig. 3 (a). The gap breaks the symmetric

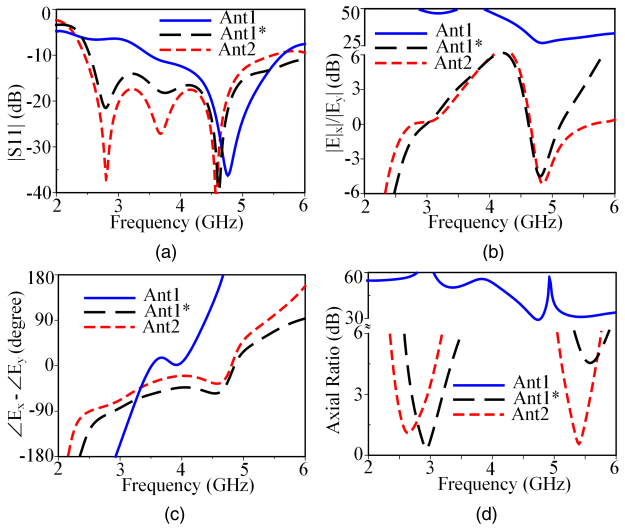

FIGURE 3. Simulated results of Stage A's antenna performance: (a) S11, (b) amplitude ratio ($|E_x|/|E_y|$), (c) phase difference ($\angle E_x - \angle E_y$), (d) axial ratio.

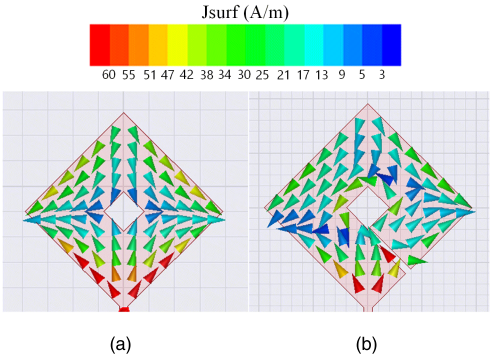

FIGURE 4. Simulated surface current distributions at 4.8 GHz for (a) Ant1 (b) Ant1* (Ant1 with gap only).

surface current distribution, thus generating the surface current in horizontal direction as shown in Fig. 4 (b). Evidently, the surface currents in horizontal and vertical directions, J_y and J_x, respectively, are balanced. The electric fields E_x and E_y can then be generated in far-field directions. Thus, APR ($|E_x|/|E_y|$) is significantly reduced as shown in Fig. 3 (b). In this study for Ant1*, the open-loop square-ring antenna has a large width. Thus, the surface currents strongly concentrate near the inner and outer edges having different current paths, which excite two CP modes at 2.9 and 5.6 GHz as shown in Fig. 3 (d). The length of inner and outer edges determines the frequency of CP modes, which will be discussed in the parametric study. The technique of using a gap to excite CP radiation has been investigated in [16]. It is noted that AR at 5.6 GHz does not satisfy the CP requirement and the CP modes do not cover the target application bands. Therefore, the notch is inserted with the help of improving AR behavior. As a result, APR is significantly reduced at high frequencies as shown in Fig. 3 (b). Besides, the notch increases the electric current path, thus moving the AR curves to lower frequency as shown in Fig. 3 (d). By an optimization process, the APR curves of 0 dB and the PD ($\angle E_x - \angle E_y$) curves of $\pm 90^0$ are

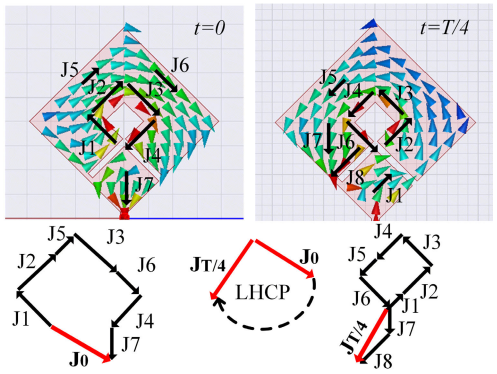

FIGURE 5. Simulated surface current distributions for Ant2 at 2.5 GHz.

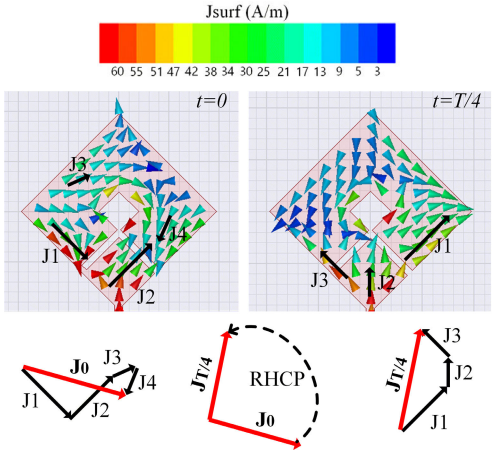

FIGURE 6. Simulated surface current distributions for Ant2 at 5.4 GHz.

obtained at 2.5 and 5.4 GHz, as shown in Figs. 3 (b) and (c), respectively. As a result, two efficient CP modes are achieved as shown in Fig. 3 (d).

To observe the sense of each CP mode, the surface current distributions at t = 0 and t = $T/4$ for both frequencies of 2.5 and 5.4 GHz are plotted where T is the time period. In Fig. 5, the intense surface current distribution flows along the inner circumference of the square-ring where the inner circumference is an approximately quarter wavelength (λ) at 2.5 GHz: $4 \cdot W_2 \approx \lambda/4$. The current sum vectors, J_0 and $J_{T/4}$, are obtained by summation of the dominant surface current vectors. Two sum vectors, J_0 and $J_{T/4}$, are noted as equal in magnitude and orthogonal in phase. The sum vector rotates clockwise, thereby generating left-hand circular polarization (LHCP) from $+z$ direction. In Fig. 6, the surface current distribution at 5.4 GHz is shown. In contrast to the CP mode at 2.5 GHz, the sense of the two current vectors, J_0 and $J_{T/4}$, rotates counter-clockwise thus producing right-hand circular polarization (RHCP) from $+z$ direction.

To sum up, Ant2 exhibits wide IBW with dual-band dual-sense CP characteristic at 2.5 and 5.4 GHz.

B. STAGE B

In this stage, Ant2 is embedded with a rhombic-shaped slot to produce Ant3. Next, the inverted V-shaped parasitic strip

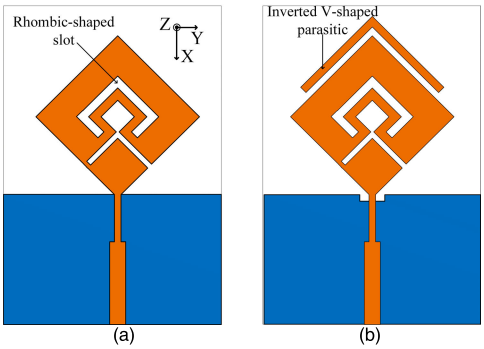

FIGURE 7. Antenna structure variations in Stage B for the additional two CP-mode generation: (a) Ant3, (b) Ant4.

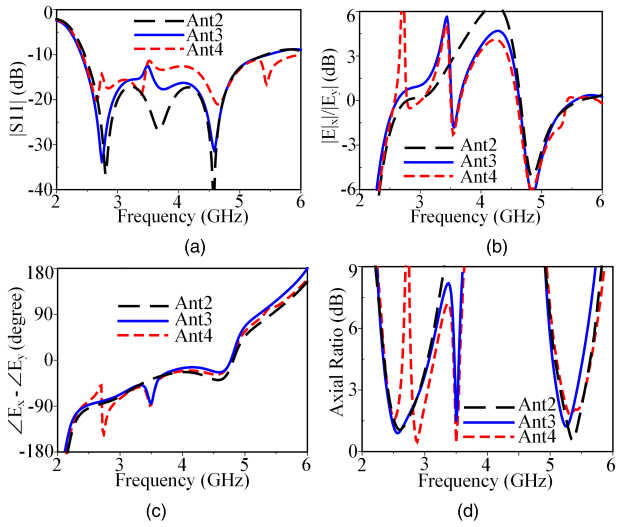

FIGURE 8. Simulated results of Stage B's antenna performance: (a) S11, (b) amplitude ratio ($|E_x|/|E_y|$), (c) phase difference ($\angle E_x - \angle E_y$), (d) axial ratio.

is added in the top of Ant3 to produce Ant4. The detailed analyses of Ant3 and Ant4 are given in the following section.

Ant3: triple-band dual-sense square-ring CP antenna embedded with a rhombic-shaped slot

In Fig. 7 (a), a rhombic-shaped slot is embedded into Ant2 producing Ant3. The dimension of the rhombic-shaped slot is defined by two parameters D_1 and D_2 as shown in Fig. 1. Due to the presence of rhombic-shaped slot, an additional resonant mode is excited around 3.3 GHz as shown in Fig. 8 (a). By a similar mechanism as the CP mode at 2.5 GHz, the rhombic-shaped slot is used to balance the current in vertical and horizontal directions at the middle frequency region. As a result, APR at the middle frequency is significantly reduced and equals 0 dB at 3.5 GHz, as shown in Fig. 8 (b). As in Fig. 8 (c), PD of 90° is also achieved at 3.5 GHz, and thus an additional CP mode is excited as shown in Fig. 8 (d).

The sense of CP mode at 3.5 GHz is determined by observing the current distributions shown in Fig. 9. The current sum vectors at t = 0 and t = *T/4* illustrate a clockwise sense of rotation, thereby generating LHCP from $+z$ direction.

Ant4: quad-band dual-sense square-ring CP antenna with an added inverted V-shaped parasitic

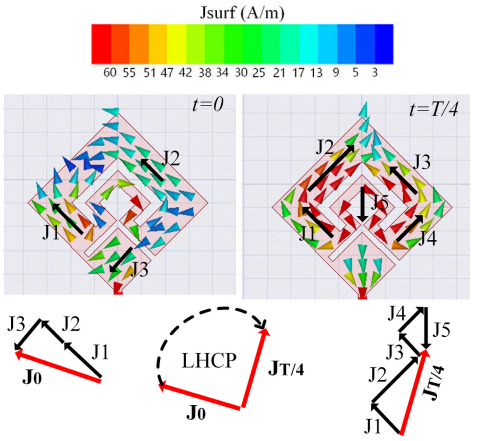

FIGURE 9. Simulated surface current distributions for Ant3 at 3.5 GHz.

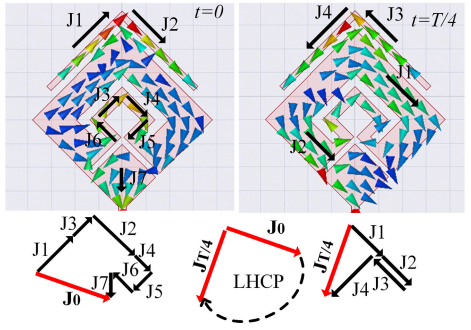

FIGURE 10. Simulated surface current distributions for Ant4 at 2.9 GHz.

In Ant4, a parasitic element is applied to excite an additional CP mode [17]–[19]. An inverted V-shaped parasitic strip is added in the top of the square-ring as shown in Fig. 7 (b). Due to the presence of the inverted V-shaped parasitic, the radiation of the square-ring is somewhat degraded. As a result, the IBW does not fully cover 3-dB ARBWs. As presented in [20], the upper edge frequency of IBW strongly depends on the feed gap (L_3). By embedding a $W_n \times L_n$ notch into the ground plane, the coupling between the lower edge of the proposed antenna and the ground plane is adjusted, thus improving IBW at the high frequency region. Besides, APR is slightly reduced at a low frequency of around 3GHz by embedding the inverted V-shaped parasitic strip. At 2.9 GHz, APR and PD are approximately 0 dB and 90° as shown in Figs. 8 (b) and (c), respectively. As a result, a new CP mode is excited at 2.9 GHz as shown in Fig. 8 (d).

The Ant4 surface current distribution at 2.9 GHz is shown in Fig. 10. The intense surface currents on the inverted V-shaped parasitic flow from one arm to the other arm. The length of the intense current path on parasitic strip is approximately equal to λ/4 at 2.9 GHz. Additionally, two sum vectors, J_0 and $J_{T/4}$, are equal in magnitude and orthogonal in phase having clockwise rotation, thus producing LHCP waves.

In brief, the proposed antenna exhibits quad-band dual-sense CP radiation. The CP modes at 2.5. 2.9, 3.5, and

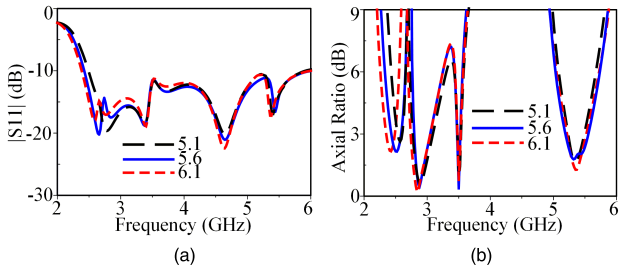

FIGURE 11. Simulated effects of varying W_2 on antenna performances: (a) S11, (b) axial ratio.

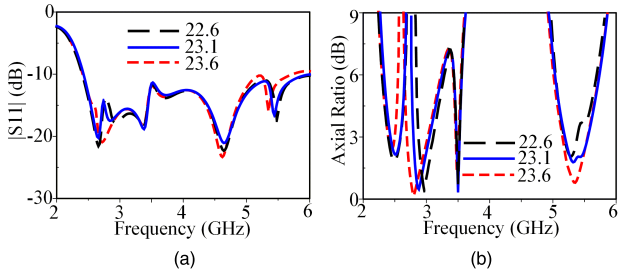

FIGURE 12. Simulated effects of varying W_3 on antenna performances: (a) S11, (b) axial ratio.

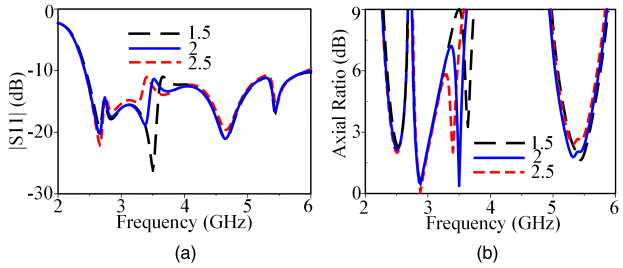

FIGURE 13. Simulated effects of varying D_2 on antenna performances: (a) S11, (b) axial ratio.

5.4 GHz are independently controlled by the key parameters of W_2, W_3, D_2, and W_1, respectively. The optimized parameters of the proposed antenna are listed as follows: $D_1 = 2.1$, $D_2 = 2$, $D_3 = 1.3$, $D_4 = 9.7$, $H_1 = 1.5$, $H_2 = 1.3$, $L_1 = 19.9$, $L_2 = 11.7$, $L_3 = 1.7$, $S_1 = 3.8$, $S_2 = 1.6$, $L_n = 1.5$, $W_n = 5.5$, $L_g = 30$, $W_1 = 27$, $W_2 = 5.6$, $W_3 = 22.6$, $W_4 = 15.85$ (unit: mm).

C. PARAMETRIC STUDY

In this section, the effect of key parameters on antenna performance is studied. The inner edge length (W_2), inverted V-shaped parasitic length (W_3), slot width (D_2), and outer edge length (W_1), which determine the length of the current path of each CP mode, are studied. When one parameter is varied, the others are kept as their optimized values excepting the case of W_1 and W_2. Varying W_1 and W_2change not only the outer and inner loop of the square-ring but also the length of the rhombic-shaped slot and inverted V-shaped parasitic, respectively. Therefore, H_1 and D_1 are adjusted to keep the length of inverted V-shaped strip and rhombic-shaped slot constant when varying W_1 and W_2.

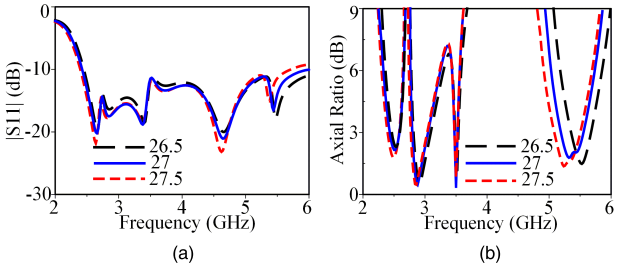

FIGURE 14. Simulated effects of varying W_1 on antenna performances: (a) S11, (b) axial ratio.

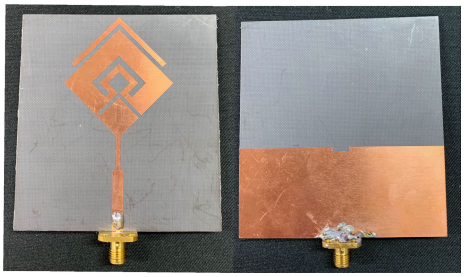

FIGURE 15. Fabricated antenna.

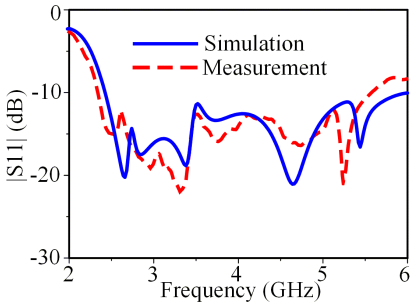

FIGURE 16. Measured result of S11.

The parametric study of W_2 on antenna performances is shown in Fig. 11. The variation of W_2 affects the CP mode at 2.5 GHz as shown in Fig. 11 (b). As W_2 increases, the inner-loop circumference increases, and thus the AR curve at 2.5 GHz moves to a lower frequency but rarely affects the other modes. The parametric study of W_3 shows that CP mode at 2.9 GHz strongly depends on the variation of parameter W_3 as shown in Fig. 12 (b). Decreasing W_3 decreases circumference of the current path on the parasitic strip, thus moving the AR curve at 2.9 GHz to a higher frequency but keeping the other CP modes unchanged. The parametric study of D_2 is shown in Fig. 13. Increasing D_2 increases the circumference of the current path around the rhombic-shaped slot thus moving the AR curve at 3.5 GHz to a lower frequency as shown in Fig. 13 (b). Meanwhile, the CP modes at other resonant frequencies are independent to the change in D_2. The parametric study of W_1 on antenna performances is shown in Fig. 14. As W_1 increases, the outer circumference of the square-ring increases, thus the AR curve at 5.4 GHz shifts to a lower frequency as shown in Fig. 14 (b). Varying W_1 strongly affects AR at the high CP mode of 5.4 GHz, while remaining unchanged at other modes.

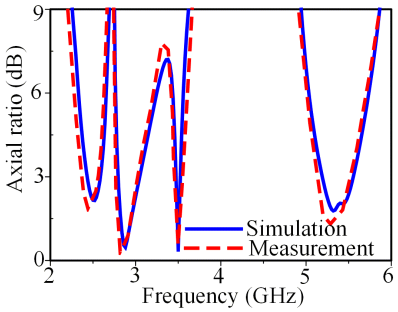

FIGURE 17. Measured axial ratio.

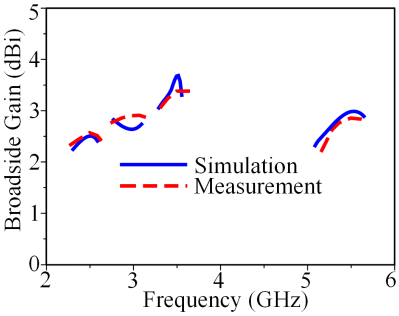

FIGURE 18. Measured gain in broadside direction.

In conclusion, the study of the key parameters shows that the CP modes of 2.5, 2.9, 3.5, and 5.4 GHz are controlled by W_2, W_3, D_2, and W_1, respectively.

III. MEASUREMENT RESULT

To validate the design principles and simulated results, the quad-band dual-sense CP antenna was fabricated. The antenna performance was verified by measuring S11 parameter using an Agilent 8720ET vector network analyzer. Meanwhile, measurement of the AR, broadside gain, and far-field radiation pattern were performed in anechoic chamber. The proposed antenna was fabricated by wet etching process as shown in Fig. 15. All of the following measured results are compared with the simulated results. Fig. 16 shows measured S11 characteristic of the fabricated antenna. The measured results yielded IBW of 83.9% (2.33-5.70 GHz), while simulated IBW was 84.4% (2.42-5.95 GHz). The measured ARBWs are shown in Fig. 17. The fabricated antenna exhibits 3-dB ARBWs of 7.3% (2.38-2.56 GHz), 9.0% (2.75-3.03 GHz), 3.7% (3.42-3.53 GHz), and 7.1% (5.16-5.54 GHz), compared to the simulated ARBWs of 7.2% (2.40-2.58 GHz), 8.9% (2.79-3.05 GHz), 2.3% (3.45-3.53 GHz), and 6.9% (5.19-5.56 GHz) showing good agreement. The measured gain in broadside direction is shown in Fig. 18. The peak gains were achieved within four distinct ARBW of 2.5, 2.9, 3.4, and 2.7 dBi, respectively.

Fig. 19 plots the measured far-field radiation patterns for the x-z and y-z planes at 2.5, 2.9, 3.5, and 5.4 GHz showing that the proposed antenna radiates LHCP at 2.5, 2.9, and 3.5 GHz and RHCP at 5.4 GHz in the $+z$ direction. Note that the major polarization gain of a CP antenna in broadside direction is considered as co-polarization and the minor one

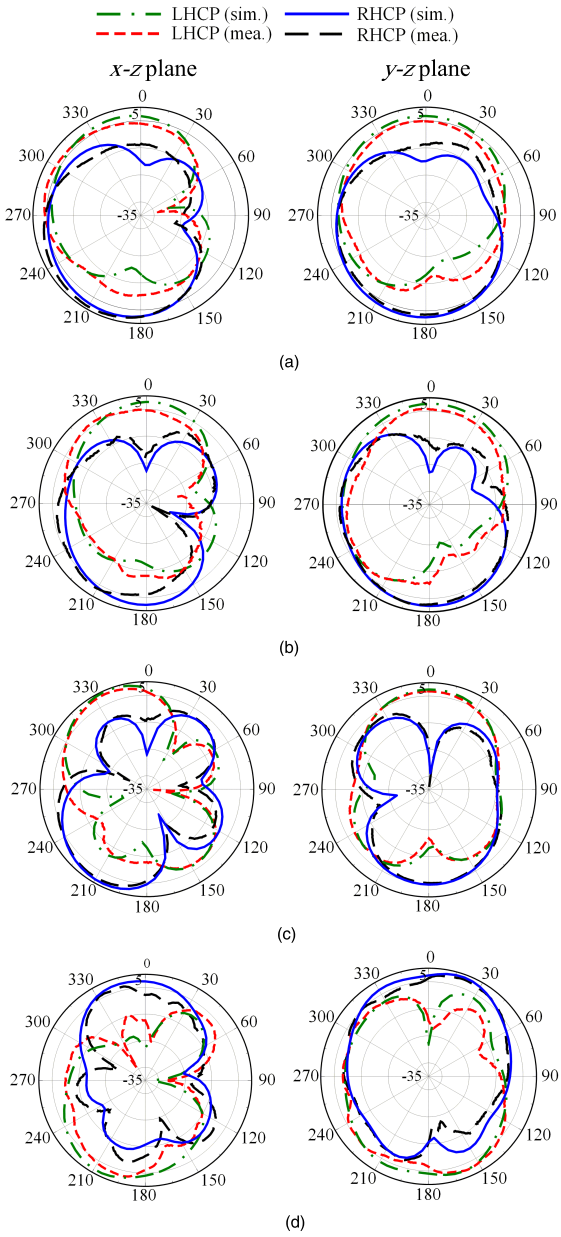

FIGURE 19. Radiation patterns of the proposed antenna for x-z and y-z planes at (a) 2.5, (b) 2.9, (c) 3.5, (d) 5.4 GHz.

is considered as cross-polarization. In the proposed antenna, LHCP is considered as co-polarization and RHCP is considered as cross-polarization at 2.5, 2.9, and 3.5 GHz. Meanwhile, at 5.4 GHz, RHCP is considered as co-polarization and LHCP is considered as cross-polarization. The measured cross-polarization discriminations in two principle planes at four CP modes range from 9 to 36 dB in broadside direction. In addition, the proposed antenna is a bi-directional radiator with somewhat distorted radiation patterns in x-z plane. This phenomenon is explained by the asymmetry of the antenna configuration in x-z plane.

Table 1 shows comparison of the proposed antenna with previous quad-band CP antennas in [5], [6], including antenna size, IBW, four distinct CP bands, and dual-sense operation.

TABLE 1. Performance comparison with other quad-band CP antennas.

Ref.	Antenna Size (λ_0^3)	IBW (%)		1st CP band (%)	2nd CP band (%)	3rd CP band (%)	4th CP band (%)	Dual-Sense Operation
[5]	1.05 × 1.05 × 0.25	14.8	80.7	5.4	8.3	3.7	2.9	No
[6]	N/A	55.4		1.0	4.3	0.9	1.4	No
Proposed	0.59 × 0.51 × 0.01	83.9		7.3	9.0	3.7	7.1	Yes

λ_0: wavelength in free space at the lowest CP frequency.

The proposed antenna achieves a wider range of ARBW at four distinct CP bands and a smaller size, compared to [5]. In addition, the proposed design is the first planar quad-band CP antenna presenting dual-sense CP characteristic by using the simple structure of a corner-fed open-loop square-ring loaded with a rhombic-shaped slot and an inverted V-shaped parasitic.

IV. CONCLUSION

In this study, a systematic design of a quad-band dual-sense CP antenna is presented. The corner-fed open-loop square-ring radiator is realized as a main radiator which generates dual-band dual-sense CP radiation. Later, a rhombic-shaped slot and an inverted V-shaped parasitic strip are used to excite two other modes. The CP principle is illustrated by the amplitude ratio and phase difference. The sense of the polarization is proved by simulation of the surface current distribution. The parametric study shows the effect of key parameters on the antenna performances. The proposed antenna was then measured, and characteristics of wide IBW and ARBW, bi-directional radiation, and dual-sense CP over quad bands resulted. Simulated and measured data agreed well. The fabricated antenna has a small volume due to the planar and simple structure. The proposed antenna is suitable for multi-functional wireless applications such as WLAN, WiMAX, and Marine Service.

REFERENCES

[1] T. V. Hoang and H. C. Park, "Very simple 2.45/3.5/5.8 GHz triple-band circularly polarised printed monopole antenna with bandwidth enhancement," *Electron. Lett.*, vol. 50, no. 24, pp. 1792–1793, Nov. 2014.
[2] R. S. Brar, K. Saurav, D. Sarkar, and K. V. Srivastava, "A triple band circular polarized monopole antenna for GNSS/UMTS/LTE," *Microw. Opt. Technol. Lett.*, vol. 59, no. 2, pp. 298–304, Feb. 2017.
[3] J. G. Baek and K. C. Hwang, "Triple-band unidirectional circularly polarized hexagonal slot antenna with multiple L-shaped slits," *IEEE Trans. Antennas Propag.*, vol. 61, no. 9, pp. 4831–4835, Sep. 2013.
[4] X. L. Bao and M. J. Ammann, "Printed triple-band circularly polarised antenna for wireless systems," *Electron. Lett.*, vol. 50, no. 23, pp. 1664–1665, Nov. 2014.
[5] T. V. Hoang, T. T. Le, Q. Y. Li, and H. C. Park, "Quad-band circularly polarized antenna for 2.4/5.3/5.8-GHz WLAN and 3.5-GHz WiMAX applications," *IEEE Antennas Wireless Propag. Lett.*, vol. 15, pp. 1032–1035, Oct. 2016.
[6] D. K. Singh, B. K. Kanaujia, S. Dwari, G. P. Pandey, and S. Kumar, "Novel quad-band circularly polarized capacitive-fed microstrip antenna for C-band applications," *Microw. Opt. Technol. Lett.*, vol. 57, no. 11, pp. 2622–2628, Nov. 2015.
[7] R. K. Saini, S. Dwari, and M. K. Mandal, "CPW-Fed dual-band dual-sense circularly polarized monopole antenna," *IEEE Antennas Wireless Propag. Lett.*, vol. 16, pp. 2497–2500, 2017.
[8] R. Xu, J.-Y. Li, J. Liu, S.-G. Zhou, K. Wei, and Z.-J. Xing, "A simple design of compact dual-wideband square slot antenna with dual-sense circularly polarized radiation for WLAN/Wi-Fi communications," *IEEE Trans. Antennas Propag.*, vol. 66, no. 9, pp. 4884–4889, Sep. 2018.
[9] R. Xu, J.-Y. Li, J. Liu, S.-G. Zhou, and K. Wei, "Design of spiral slot-based dual-wideband dual-sense CP antenna," *IET Microw. Antennas Propag.*, vol. 13, no. 1, pp. 76–81, Jan. 2019.
[10] A. Altaf and M. Seo, "A tilted-D-shaped monopole antenna with wide dual-band dual-sense circular polarization," *IEEE Antennas Wireless Propag. Lett.*, vol. 17, no. 12, pp. 2464–2468, Dec. 2018.
[11] R. Xu, J. Li, Y.-X. Qi, Y. Guangwei, and J.-J. Yang, "A design of triple-wideband triple-sense circularly polarized square slot antenna," *IEEE Antennas Wireless Propag. Lett.*, vol. 16, pp. 1763–1766, 2017.
[12] T. T. Le and H. C. Park, "Very simple circularly polarised printed patch antenna with enhanced bandwidth," *Electron. Lett.*, vol. 50, no. 25, pp. 1896–1898, Dec. 2014.
[13] T. V. Hoang, T. T. Le, Q. Y. Li, and H. C. Park, "Penta-band circularly polarised antenna using a lumped capacitor," *IET Microw. Antennas Propag.*, vol. 10, no. 8, pp. 856–862, May 2016.
[14] M. Midya, S. Bhattacharjee, and M. Mitra, "Broadband circularly polarized planar monopole antenna with g-shaped parasitic strip," *IEEE Antennas Wireless Propag. Lett.*, vol. 18, no. 4, pp. 581–585, Apr. 2019.
[15] S. I. Latif and L. Shafai, "Polarisation and resonant characteristics of gap-loaded microstrip square ring antennas," *IET Microw. Antennas Propag.*, vol. 4, no. 6, pp. 733–742, Jun. 2010.
[16] R.-L. Li, V. F. Fusco, and H. Nakano, "Circularly polarized open-loop antenna," *IEEE Trans. Antennas Propag.*, vol. 51, no. 9, pp. 2475–2477, Sep. 2003.
[17] J. Wu, Y. Yin, Z. Wang, and R. Lian, "Broadband circularly polarized patch antenna with parasitic strips," *IEEE Antennas Wireless Propag. Lett.*, vol. 14, pp. 559–562, 2015.
[18] K. Ding, C. Gao, D. Qu, and Q. Yin, "Compact broadband circularly polarized antenna with parasitic patches," *IEEE Trans. Antennas Propag.*, vol. 65, no. 9, pp. 4854–4857, Sep. 2017.
[19] K. Ding, C. Gao, Y. Wu, D. Qu, and B. Zhang, "A broadband circularly polarized printed monopole antenna with parasitic strips," *IEEE Antennas Wireless Propag. Lett.*, vol. 16, pp. 2509–2512, 2017.
[20] M. J. Ammann, "Impedance bandwidth of the square planar monopole," *Microw. Opt. Technol. Lett.*, vol. 24, no. 3, pp. 185–187, Feb. 2000.

TU TUAN LE received the B.S. degree in electronics and telecommunications from the Hanoi University of Science and Technology, Hanoi, Vietnam, in 2013, and the Ph.D. degree from the Department of Electronics and Electrical Engineering, Dongguk University, Seoul, South Korea. He is currently with Hanyang University, Seoul, as a Postdoctoral Research Fellow. His current research interests include RF energy harvesting, wearable antennas, circularly polarized antennas, reconfigurable antennas, and multiband/broadband planar antennas for various wireless applications.

TAE-YEOUL YUN received the Ph.D. degree from the Department of Electrical Engineering, Texas A&M University, College Station, TX, USA, in 2001. From 1989 to 1996, he was with the Optical Telecommunication System Group, ETRI, Daejeon, South Korea, where he developed 2.5- and 10-Gb/s systems. From 2001 to 2003, he was an MMIC Designer with Triquint Semiconductor, Dallas, TX, USA. Since 2003, he has been a Professor with Hanyang University, Seoul, South Korea. His research interests include RFICs, antennas, and wireless/optical high-speed communication systems.